Available online at www.sciencedirect.com
SCIENCE DIRECT
Journal of Power Sources 153 (2006) 265–273
JOURNAL OF POWER SOURCES
www.elsevier.com/locate/jpowsour

Lithiation of ramsdellite–pyrolusite MnO_2; NMR, XRD, TEM and electrochemical investigation of the discharge mechanism

W. Bowden [a,*], C.P. Grey [b], S. Hackney [c], F. Wang [a], Y. Paik [b], N. Iltchev [a], R. Sirotina [a]

[a] *Gillette Technology Center, US, Needham MA, USA*
[b] *SUNY Stony Brook, NY, USA*
[c] *Michigan Technological University, Houghton MI, USA*

Available online 11 July 2005

Abstract

Electrolytic manganese dioxide (EMD) is made in aqueous sulfuric acid and neutralized or ion exchanged with aqueous lithium hydroxide before use in Li batteries. Solid state Li NMR studies show that Li is present on surface and vacancy sites and migrates into Mn (III) related sites after heat treatment to remove water. During heat treatment the MnO_2 rearranges from ramsdellite/pyrolusite intergrowth EMD to a defect pyrolusite heat-treated manganese dioxide (HEMD). EMD exhaustively treated with lithium hydroxide solution has 40–50% of the protons in EMD exchanged for Li ions to produce a structurally unchanged γ-MnO_2. Li magic angle spinning (MAS) NMR reveals that this lithiated material contains lithium in cation vacancy and Mn (III) related sites in the MnO_2 lattice in addition to ionic Li on the surface. During heat treatment, the vacancy lithium content prevents the ramsdellite to pyrolusite rearrangement in HEMD formation. Instead, an ordered ramsdellite/pyrolusite intergrowth of lithiated manganese dioxide (LiMD) is formed with an approximate composition of 50% ramsdellite and 50% pyrolusite. Li MAS NMR of LiMD shows Li resonances near 280 and 560 ppm, consistent with Li transition from surface and cation vacancy sites into the ramsdellite lattice.

LiMD discharged against lithium shows two processes, one near 3.1 V, the other about 2.8 V. Li MAS NMR studies show the initial reduction results a lithium resonance near 560 ppm associated with Li near a mixed valence Mn (III/IV) environment followed by appearance of a resonance near 100 ppm consistent with a Li environment near Mn (III). TEM studies of the reduced material show initial expansion of the ramsdellite lattice accompanied by a loss in crystallinity in the 3.1 V discharge process followed by disappearance of the pyrolusite content via conversion to ramsdellite in the second discharge process.

Keywords: Manganese dioxide; Lithiation; Ramsdellite; Pyrolusite; Li NMR; CBED

1. Introduction

Lithium/manganese dioxide batteries are a high energy density, high drain power source used when the need for high power, voltage and calendar life justifies the comparatively high cost of the cell. Initial efforts to use manganese dioxide as the cathode active material in a nonaqueous lithium battery were unsuccessful owing to gassing caused by the high moisture content of commercial γ-phase manganese dioxides. Ikeda found that heating the manganese dioxide above 300 °C to remove moisture produced an electrochemically active form of manganese dioxide with acceptable gassing [1,2]. Detailed investigation showed the heat-treated manganese dioxide, known as HEMD, was mainly a disordered pyrolusite material formed by rearrangement of the ramsdellite MnO_2 in the ramsdellite/pyrolusite intergrowth of the parent γ-manganese dioxide [3–5]. On discharge, pyrolusite is lithiated in an irreversible process followed by insertion of additional lithium in a reversible process [4,5]. Electrochemical lithiation of HEMD was studied by X-ray diffraction, transmission electron microscopy (TEM) and magic angle spinning (MAS) solid state NMR to reveal that the initial irreversible process was lithiation of the defect

* Corresponding author. Tel.: +1 781 292 8530; fax: +1 781 292 8615.
E-mail address: bill_bowden@gillette.com (W. Bowden).

0378-7753/$ – see front matter © 2005 Elsevier B.V. All rights reserved.
doi:10.1016/j.jpowsour.2005.05.059

pyrolusite with a lattice rearrangement to recreate a ramsdellite lattice followed by additional lithiation of the ramsdellite [5,6].

It was found that a more stable cell resulted if the sodium content of manganese dioxide was be replaced by treatment with acid followed by LiOH solution prior to heat treatment [7,8]. Exhaustive treatment of the MnO_2 with LiOH solution or mechano-chemical lithiation conditions resulted in more extensive lithium incorporation into the MnO_2. After heat treatment, a new manganese dioxide phase, referred to as LiMD was formed [9–11].

The structure of lithiated manganese dioxide (LiMD) and its lithiation products has been examined by ^{6}Li MAS NMR spectroscopy, XRD, TEM and convergent beam electron diffraction (CBED) to characterize the material. The electrochemical lithiation of LiMD was studied by discharge in 2430 size coin cells and 2/3A wound cells both by constant current and stepped potential discharge methods [12,13]. Results of these investigations are discussed below.

2. Experimental

2.1. Preparation of LiMD

In a typical experiment, 800 g electrolytic manganese dioxide (Kerr-McGee Chemical Co.) was dispersed in about 1500 cc distilled water with vigorous stirring and 300 cc 3 M sulfuric acid was added. After about 1 h, the stirring was terminated and the MnO_2 settled to the bottom. The supernatant sulfuric acid solution, now containing the ion exchangeable sodium from the MnO_2 was decanted, the MnO_2 washed once with 1500 cc water and then once more dispersed in 1500 cc water. Solid $LiOH{\cdot}H_2O$ was then gradually added to the stirred suspension. With addition of the LiOH, the MnO_2 suspension became a chocolate color as the MnO_2 peptized, and then became darker as the MnO_2 re-agglomerated. After about 120 g $LiOH.H_2O$ has been added and a pH of about 12.5 achieved, the MnO_2 was allowed to stand overnight. The lithiated MnO_2 was isolated by filtration and dried overnight at 110 C to produce a dark free-flowing powder. The lithiated MnO_2 was then heated in air to 350 C for 7 h to form LiMD. LiMD synthesized by this procedure varies from 0.75–0.90% Li.

2.2. Experimental methods

Electrochemical results were obtained from 2430 size crimp-sealed coin cells. Cells were modified to assure cathode limited construction. Cathodes were formed by mixing a composition of 60% MnO_2, 30% graphite (KS-6) and 10% Teflon powder in a blender and then by pressing a cathode pellet containing about 300 mg active material into the can. Limited experimental results were also gained in 2/3A size wound cylindrical cells.

The can-cathode assemblies were dried under vacuum in a dry room (<2% r.h.) and then vacuum filled with electrolyte (EC/PC/DME/LiTFS) and crimped in the dry room.

SPECS discharges were performed with an Arbin multichannel potentiostat at stepping rate of 5 mV each hour and 5 mV every 2 h, while cell discharges were done using a Maccor battery test system.

Cells were disassembled in an argon-filled glove box.

Li MAS NMR experiments were performed on a CMX-200 spectrometer with a Chemagnetics probe equipped with a 4 mm probe for MAS. Spectra were recorded using a rotor synchronized Hahn-echo pulse sequence. The X-ray diffraction scans were carried out on a Scintag XDS 2000 or Siemens diffractometer using Cu Kα radiation and a scanning rate of 0.01° (2θ) per second. The samples were prepared by packing powders of MnO_2 into aluminum holders covered by a glass slide, producing a dense agglomerate of powder with a macroscopically flat surface suitable for X-ray diffraction studies. Transmission electron imaging and diffraction studies were carried out using a JEOL 4000 operated at 200 KV. Convergent beam electron diffraction was carried out using a beam size between 5 and 10 nm. The specimens were prepared by collecting EMD powder particles on discontinuous carbon films. This approach allowed for examination of EMD powder without prior exposure to heat, vacuum and heavy ion irradiation associated with ion milling techniques.

3. Results

3.1. Characterization of lithiated manganese dioxide

Fig. 1 compares the XRD pattern of manganese dioxide after three treatments. Firstly, the X-ray diffraction patterns of the lithium hydroxide treated EMD (a) is shown and is identical to that of untreated EMD. Secondly, the XRD pattern of HEMD (b) is shown and is characterized by a peak at 28° characteristic of pyrolusite and a second peak near 58°. Thirdly, the XRD pattern of lithiated manganese dioxide (c)

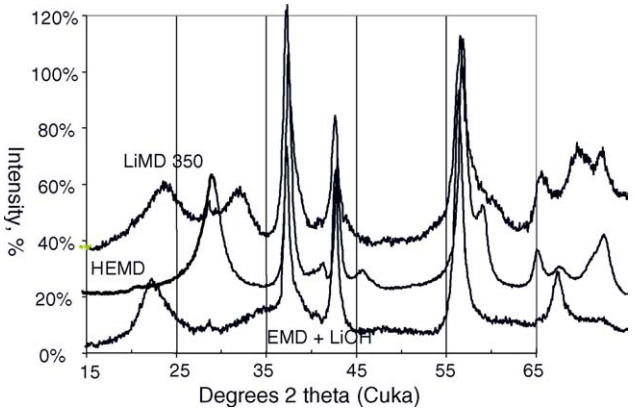

Fig. 1. X-ray diffraction patterns of EMD after treatment with LiOH (γ-MnO_2), HEMD (β-MnO_2) and LiMD.

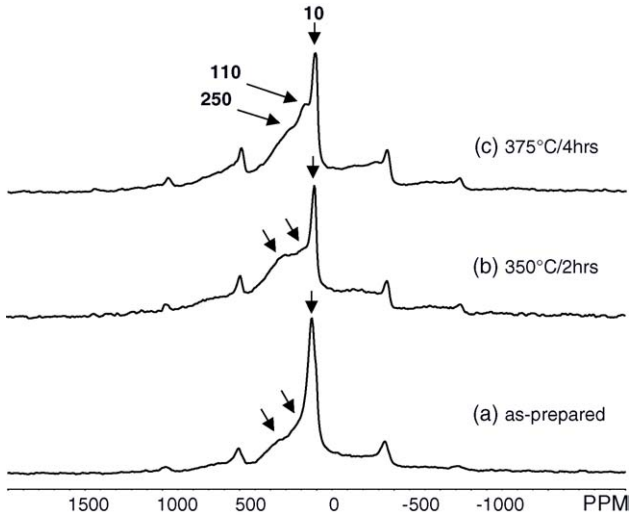

Fig. 2. ^{6}Li MAS NMR spectrum of LiOH neutralized EMD (at pH 7) and after conversion to HEMD.

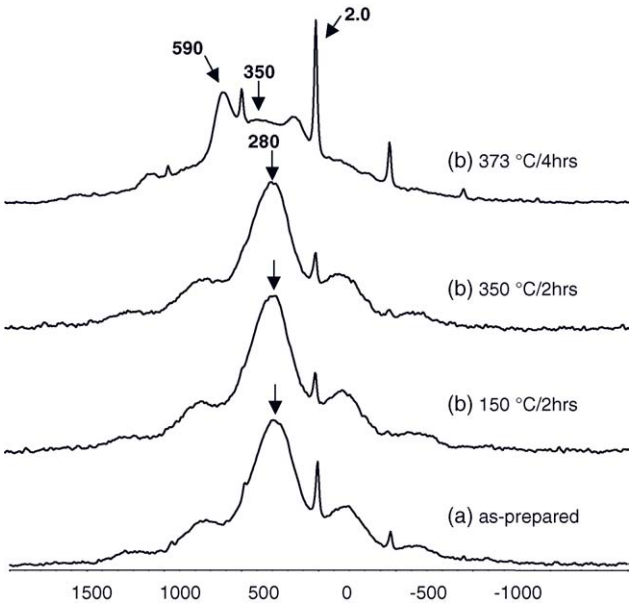

Fig. 3. ^{6}Li MAS NMR spectrum of EMD follwing pH 12.5 lithiation and after heat treatment.

is characterized by two peaks, one near 24 and the other near 32° 2θ. The EMD and LiMD patterns have a small peak at 28° from a pyrolusite impurity. The LiMD peak near 24° is though to arise from the ramsdellite 1 1 0 seen near 22° in EMD and the peak near 32° from a shift of the broad peak found near 35° in the EMD pattern. The lithiated MnO_2 material depicted in Fig. 1 differs significantly from CDMO. The Lix-MnO_2 material studied by Nohma et al. [14,15] is described as "a composite oxide of gamma/beta MnO_2 and Li_2MnO_3" and was described as a composite dimensional manganese oxide (CDMO). Most of the Nohma et al. studies focused on materials formed by heat treating Li salts with EMD at Li/Mn ratios at 3/7 with some consideration of lower Li/Mn ratios. The electrochemistry studies of these materials indicated an initial discharge capacity less than 0.20 Ah g^{-1}. This initial discharge capacity is significantly lower than that reported for the LiMD materials studied in this paper (Fig. 4). The Li/Mn = 3/7 CDMO materials show XRD patterns having intensities that correspond to Li_2MnO_3 peak positions at 18° and 45° 2θ. These peaks are not observed in the XRD patterns for the materials reported in this paper (Fig. 1).

The ^{6}Li MAS NMR spectrum of LiOH treated EMD is shown in Fig. 2.

As shown in the figure there is a common resonance near 10 ppm ascribed to Li in environments where the Li^+ is not directly (or only weakly) coordinated to the MnO_2 oxygen atoms of the surface or in the macropores, e.g., as hydrated Li^+ ions. The broad resonances near 110 and 250 ppm that become somewhat more prominent after heating are assigned to Li near octahedral Mn (III) (110 ppm) and Li in cation vacancy sites and tightly bound surface sites (250 ppm). Note that the Mn (III) peak is only clearly visible following heat treatment at 350 °C. The MAS NMR shows that, at near neutral pH, the Li environment is dominated by weakly bound Li^+ ions that are not shifted by proximity to paramagnetic Mn ions. The contrast to the ^{6}Li MAS NMR of EMD lithiated to pH 12.5, shown in Fig. 3 below, is instructive.

In Fig. 3, the weak resonance near 2 ppm is again assigned to ionic lithium. The resonance at near 280 ppm is again assigned to Li in a cation vacancy site, and is now much stronger than at the lower pH. On continued heating to 375 C, a resonance appears indicating Li in a mixed valence Mn (III/IV) environment in the 2 × 1 tunnels at 590 ppm. The resonance due to lithium in cation vacancy sites near 280 ppm becomes less intense and shifts slightly to 350 ppm indicating both destruction of some of the vacancy sites and an alteration of their environment.

The electrochemistry of LiMD was determined in the 2430 size coin cell. The results on 100-h discharge are shown in Fig. 4 below and are compared to those for HEMD derived from the same parent EMD. As shown in the figure, the

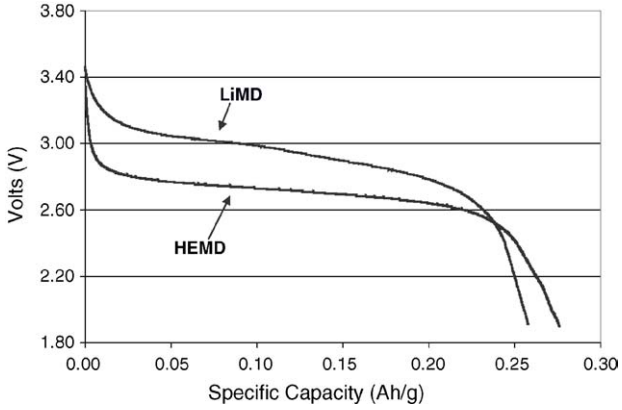

Fig. 4. Comparison of discharge curves of HEMD and LiMD at the 100 h rate showing the higher voltage of LiMD.

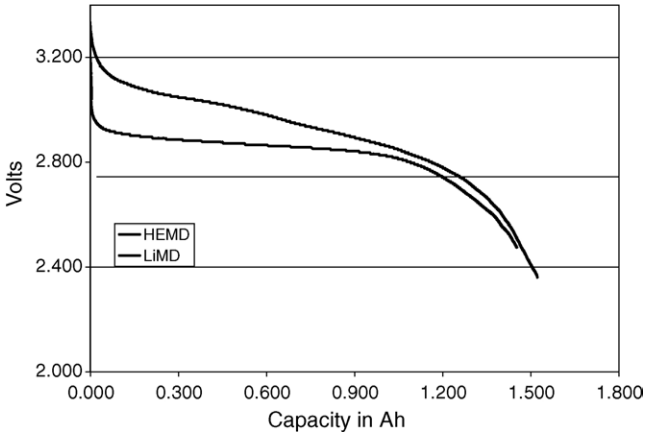

Fig. 5. Comparison of capacity and running voltage of HEMD and LiMD on low rate (100 h) discharge in 2/3 A cells.

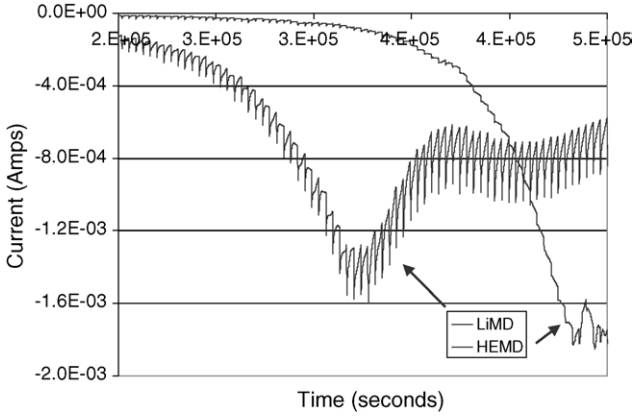

Fig. 6. SPECS discharge of LiMD and HEMD compared, showing the initial reversible lithium insertion in LiMD followed by a second reduction compared to the irreversible reduction process in HEMD.

discharge voltage of LiMD is significantly higher than a comparable HEMD material.

Even though the capacity of the LiMD was marginally lower than HEMD and the measured density was slightly

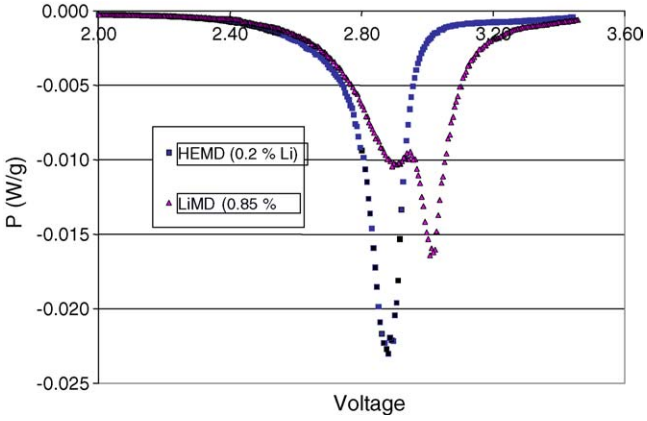

Fig. 7. Comparison of power vs. voltage for HEMD and LiMD showing two discharge processes for LiMD, one a higher voltage and one superimposable with HEMD.

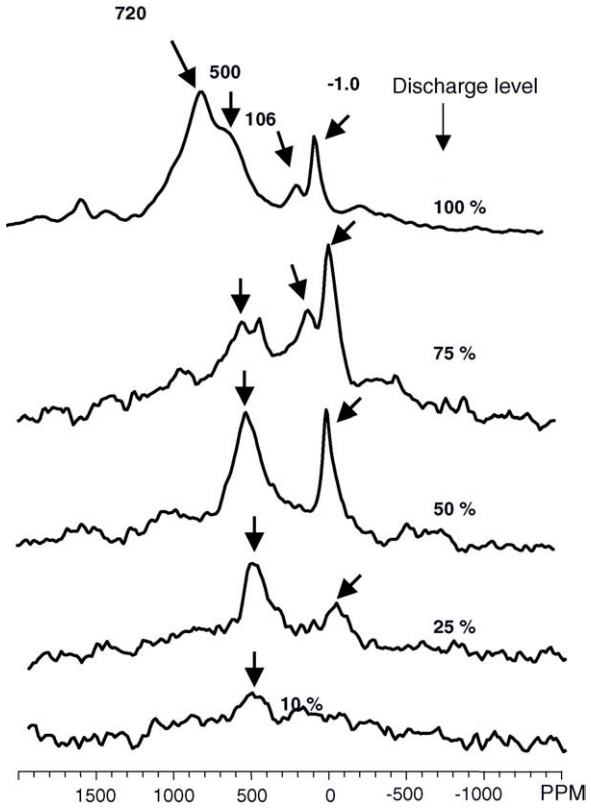

Fig. 8. ^{6}Li MAS NMR of LiMD cathodes from 2430 cells showing an increase and decline near 500 ppm and an increase near 100 ppm as depth of discharge increases.

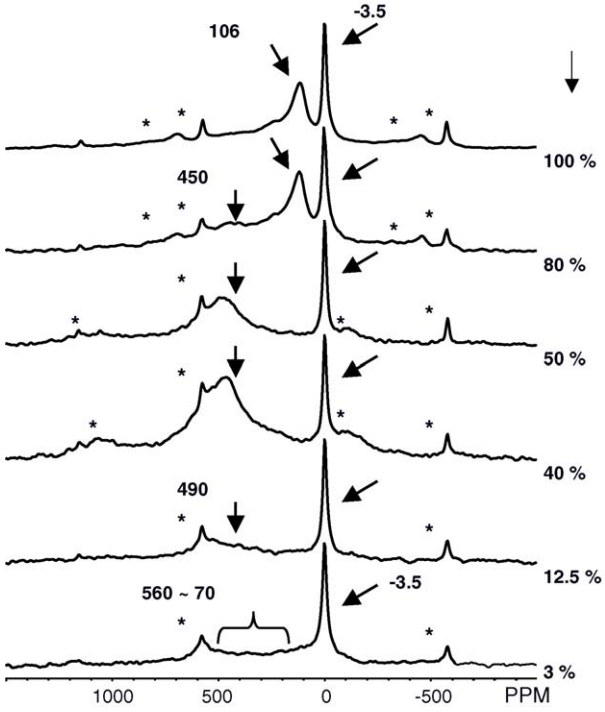

Fig. 9. ^{6}Li MAS NMR of cathode HEMD materials removed from partly discharged 2/3A Li/MnO_2 cells. Asterisks indicate spinning sidebands.

lower at 4.43 g cm^{-3} versus 4.77 g cm^{-3} for HEMD, the capacity in 2/3A size cells was very similar. This result, shown in Fig. 5, indicates good packing density for the LiMD and a high capacity in a volume limited cell. A slight break in the LiMD discharge curve near 3.0 V suggests there may be two discharge processes observed in the reduction of LiMD.

The discharge mechanism of LiMD and HEMD were compared using the SPECS discharge experiment. In the SPECS experiment, the cell is held at a given voltage for a set period of time and the current recorded. Behavior of current at a given voltage is a useful tool to distinguish between homogeneous (reversible) processes and non-homogeneous processes. The initial reduction of HEMD is irreversible, as previously reported by Nardi [4] and Bowden et al. [5]. This combination of an irreversible initial discharge and homogeneous second discharge process is shown in Fig. 6 below while the discharge of LiMD is reversible [11].

HEMD shows an irreversible lithiation process with a rise in current at constant voltage, consistent with an activation process [5]. In contrast, LiMD shows a reversible reduction with a smooth decline in current after each voltage step consistent with a homogeneous lithiation of the LiMD. The SPECS technique was also used to examine the discharge process in greater detail. As shown in Fig. 7, the LiMD SPECS plot of current versus voltage discloses the presence of two separate discharge processes, compared to one for HEMD. The change in local environments for Li during the discharge of LiMD was studied by discharging a series of 2430 size cells to given depth of discharge, then removing the cells from the test rack and disassembling them to allow examination of the cathodes. The local. environments of lithium in the cathode were examined by ^{6}Li MAS NMR. As shown in Fig. 8 below, the change in NMR resonance pattern during the discharge of LiMD in coin cells is reminiscent of the pattern earlier observed after post mortem analysis of 2/3 A size cells with HEMD cathodes.

As shown in Fig. 8, the discharge of LiMD initially shows a resonance near 500 ppm increasing steadily in prominence and reaching a maximum at about 50% depth of discharge. In the second half of the discharge, the resonance near 500 ppm decreases in magnitude and instead a resonance near 106 ppm becomes more prominent. The initial appearance of a 500-ppm resonance followed by a 100-ppm resonance is almost

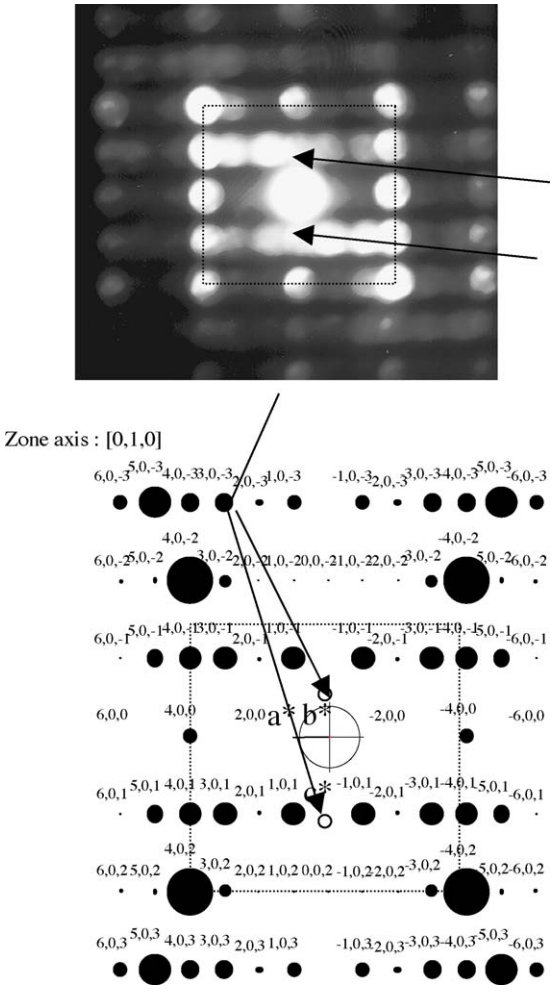

Fig. 10. Comparison of CBED pattern of 10% discharged LiMD and simulation of ramsdellite lattice. Arrows show forbidden 0 0 1 and 0 0-1 reflections.

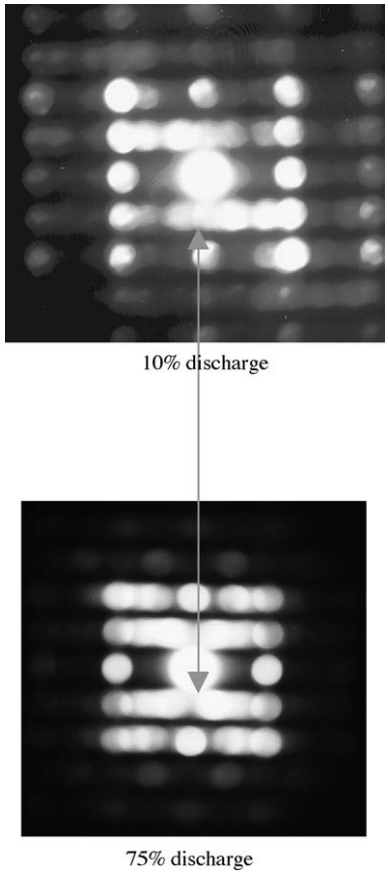

Fig. 11. Comparison of 10 and 75% discharged LiMD. Note how the intensity at the indicated 0 0 1 positions is decreased for the 75% relative to the 10% discharge. Comparison of these intensities in the 0 1 0 CBED patterns from the 10 and 75% discharge suggests a decrease in the ordering and/or a decrease in the presence of De Wolff defects.

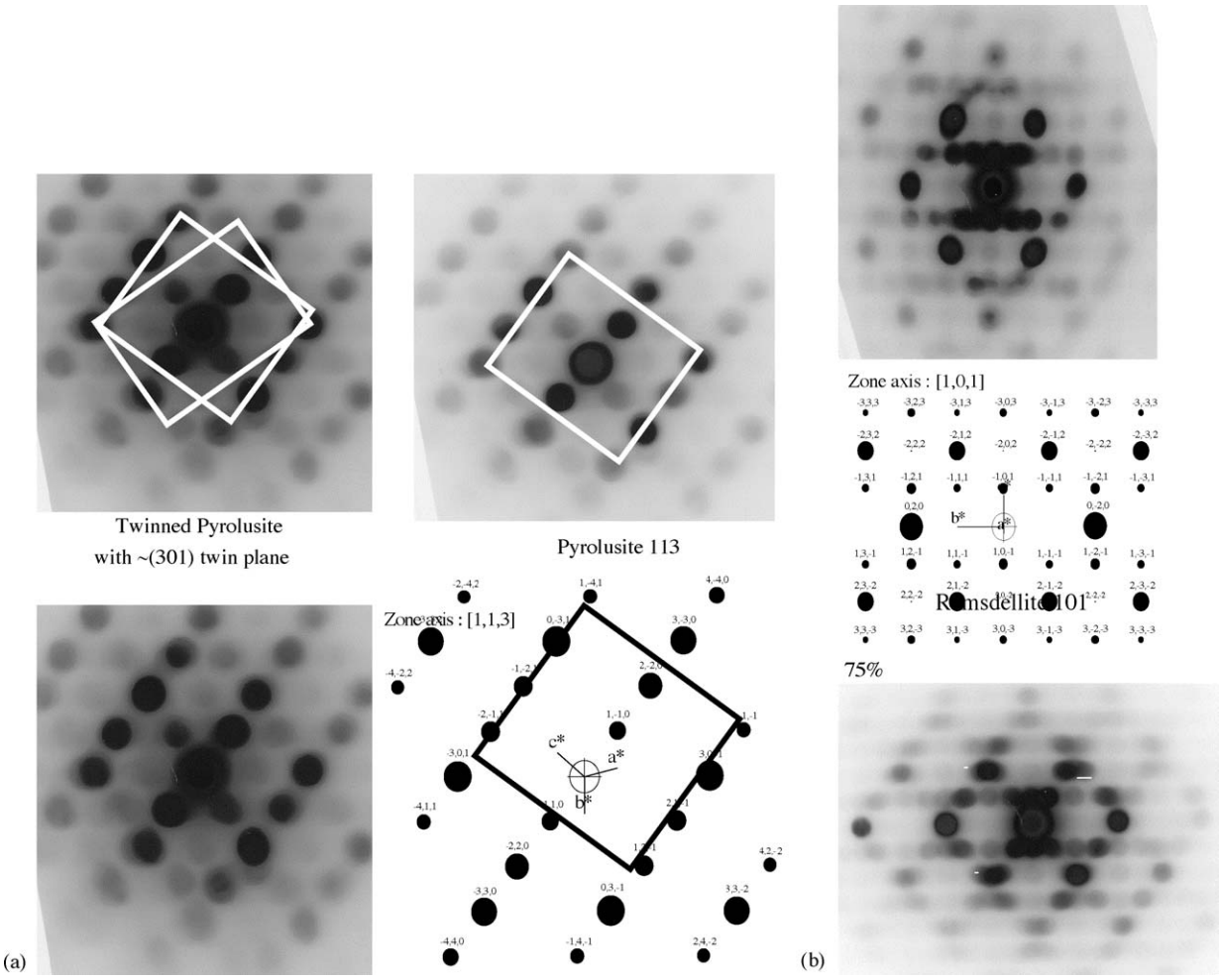

Fig. 12. (a) Interpretation of commonly observed LiMD pattern as (3 0 1) twinned pyrolusite. (b) Comparison of CBED patterns on 1 0 1 zone axis at 10 and 75% discharge. At higher discharge fractions, the lattice parameter of the topotactic ramsdellite/twinned pyrolusite structure increases, leading to a smearing of the reciprocal lattice to lower diffraction angles (arrows). As discharge occurs, ramsdellite forms a topotactic structure on the pyrolusite twin structure. The 1 0 1 zone axis simulation for ramsdellite is compared to the experimental pattern. Good fit is obtained if the pyrolusite reflections (x) are removed.

identical to the behavior of HEMD in wound cells (shown in Fig. 9).

The irreversible initial lithiation process in HEMD was interpreted as lithium insertion with rearrangement of the pyrolusite to a ramsdellite lattice [5]. Lithium in the ramsdellite unit cell was considered to lead to the mixed octahedral Mn (III/IV) environment (with a resonance at 500 ppm) initially observed. Continued lithiation of the ramsdellite would then lead to an octahedral Mn (III) site, consistent with the final NMR spectrum. The crystal structure of LiMD and subsequent structure of the discharged LiMD was studied using convergent beam electron diffraction. The CBED studies indicate LiMD is spatially non-uniform, containing both regions of De Wolff faulted crystals rich in pyrolusite or ramsdellite. The changes in the [0 1 0] ramsdellite CBED patterns upon discharge are of particular interest (Fig. 10). Consider the observed intensity at the 0 0 1 ramsdellite position. This intensity is normally forbidden by the structure factor rules for the ramsdellite crystal structure. However, it has been proposed that when a substantial concentration of De Wolff pyrolusite defects are present, then there may be some ordering of defects such that the 1×1 tunnels of pyrolusite alternate with the 2×1 tunnels of ramsdellite. This produces a new unit cell in which the intensity observed at the 0 0 1 ramsdellite position is allowed. This type of intensity, attributed to partial ordering of De Wolff defects, is also observed at $\sim 20^\circ$ 2θ (Cu) in the simulated diffraction patterns of Chabre and Pannetier [16].

There is evidence that the forbidden intensity at the 0 0 1 ramsdellite position is reduced in some crystals as the depth of discharge is increased, as shown in Figs. 11 and 12. It will be argued below that the 0 0 1 ramsdellite intensity is due to ordering of De Wolff defects at high De Wolff defect density. Thus, the reduction of intensity at the forbidden position may be interpreted as a reduction in density of De Wolff defects, creating a structure that, on average, is more similar to the 'perfect' ramsdellite structure. We note that the dimensions of the [0 1 0] ramsdellite patterns change upon

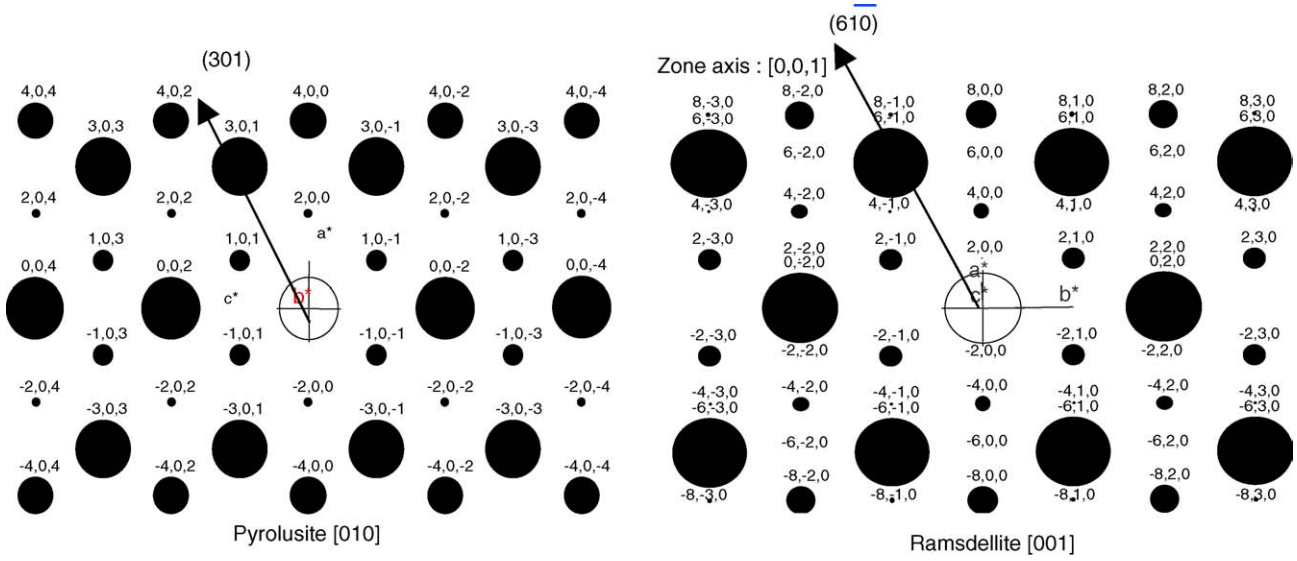

Fig. 13. Proposed reciprocal lattice relation of pyrolusite domains in LiMD with ramsdellite. The normals to the topotactic twin planes are indicated by arrow.

discharge, corresponding to a change in the ramsdellite unit cell volume. Lattice parameter data from several [0 1 0] ramsdellite CBED patterns was plotted against depth of discharge and showed experimentally significant increases in both *a* and *c* lattice parameters with increasing discharge.

The CBED patterns of pyrolusite rich regions of the LiMD material commonly show a pattern with symmetry that is difficult to index as a single crystal of pyrolusite. However, we find agreement between this observed pattern and a hypothesis of (3 0 1) twinned pyrolusite, Fig. 12a. Moreover, studies of these regions after discharge suggest a topotactic transformation of twinned.

Pyrolusite to ramsdellite with [1 1 3] pyrolusite//[1 0 1] ramsdellite has resulted from the discharge process (Fig. 12b).

It is of interest to consider the origin of the twinning in the pyrolusite rich structure of the LiMD. We examine the crystallographic relationship with the ramsdellite rich structure of the original EMD. We consider the crystallographic relationship that would occur with pyrolusite defects if the 2×1 tunnels of ramsdellite are parallel with the 1×1 tunnels of pyrolusite, as predicted by De Wolff [17,18]. If the topotactic crystal structures are viewed along 0 0 1 ramsdellite//0 1 0 pyrolusite (together with the associated reciprocal lattice planes, Fig. 13), it becomes apparent that the {6 1 0} twin planes observed for ramsdellite in EMD are parallel to the {3 0 1} twin planes observed for the pyrolusite in the LiMD. Now we must consider the transformation upon discharge of LiMD, where we have proposed an expanded ramsdellite structure is formed topotactic with the twinned pyrolusite structure. In this case, Fig. 12b suggests that the twinned pyrolusite at the <1 1 3> orientation transforms to the <1 0 1> ramsdellite, with the topotactic relationship approximated as <1 0 1>Rams//<1 1 3>Pyro; (0 2 0)Rams//(−3 0 1) Pyro.

This, however, is not the same topotactic relationship as reported in Fig. 12a. In fact, there is no parallelism between the 1×1 tunnels of pyrolusite and the 2×1 tunnels of ramsdellite in the topotactic relationship represented by Fig. 9. These results suggest that there is a hysteresis in the formation of the topotactic structures in that the transformation from LiMD ramsdellite → LiMD pyrolusite upon heating results in a different topotactic relationship than LiMD pyrolusite → LiMD ramsdellite upon discharge.

4. Discussion

4.1. Structure of LiMD

The lithium content of 0.75–0.9% distinguishes LiMD from CDMO since the CDMO has an approximate Li content

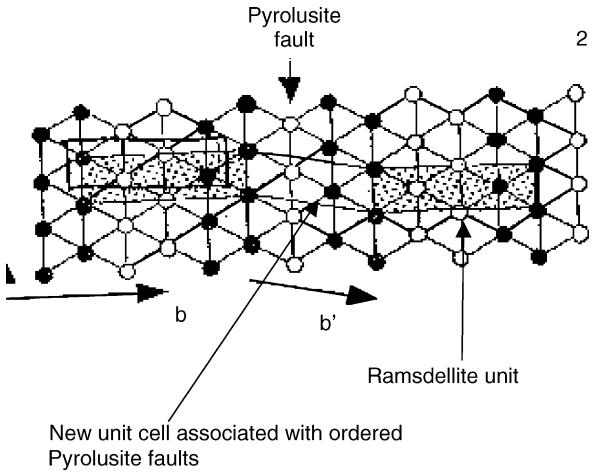

Fig. 14. Intergrowth structure consistent with that seen in LiMD XRD pattern (after Chabre and Pannetier).

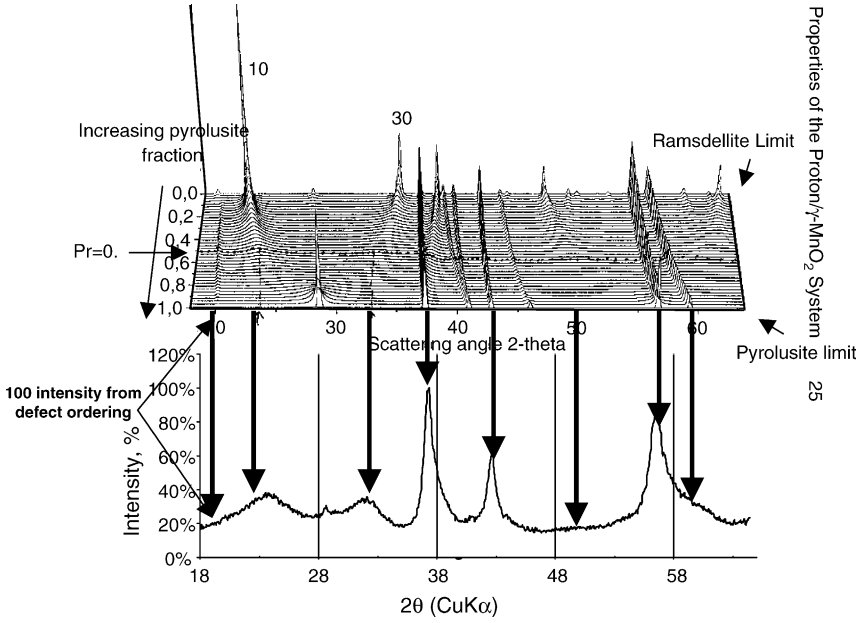

Fig. 15. Comparison of LiMD XRD pattern with DIFFAX simulation of ramsdellite pyrolusite intergrowth (adopted from Chabre and Pannetier).

of 3.2%. Structurally as well CDMO is thought to be of distorted rock salt structure while LiMD clearly belongs to the γ-MnO_2 family. We examine the XRD data for LiMD using the results of Chabre and Pannetier [16]. Chabre and Pannetier have calculated the XRD patterns of MnO_2 structures ranging from perfect (defect free) ramsdellite as a function of increasing De Wolff defects to the limiting case of perfect pyrolusite. A De Wolff defect is a defect in the ramsdellite lattice in which a layer of 1×1 tunnel structure (pyrolusite) is interspersed with the layers of the 2×1 tunnel structure of ramsdellite, as shown in Fig. 14 [16]. The XRD pattern for the LiMD 350 °C is qualitatively compared to the calculated results of Chabre and Pannetier in Fig. 15, where it is seen that the structure may be described as an approximately 50:50 mixture of layers, or intergrowth, of 2×1 and 1×1 tunnel structures. As such, it may be concluded that the materials with associated XRD patterns in Fig. 1 may be categorized by increasing pyrolusite content as EMD + LiOH 1 1 0 C < LiMD 350 C < HEMD. By contrast, the lithium containing manganese dioxide composite densified manganese

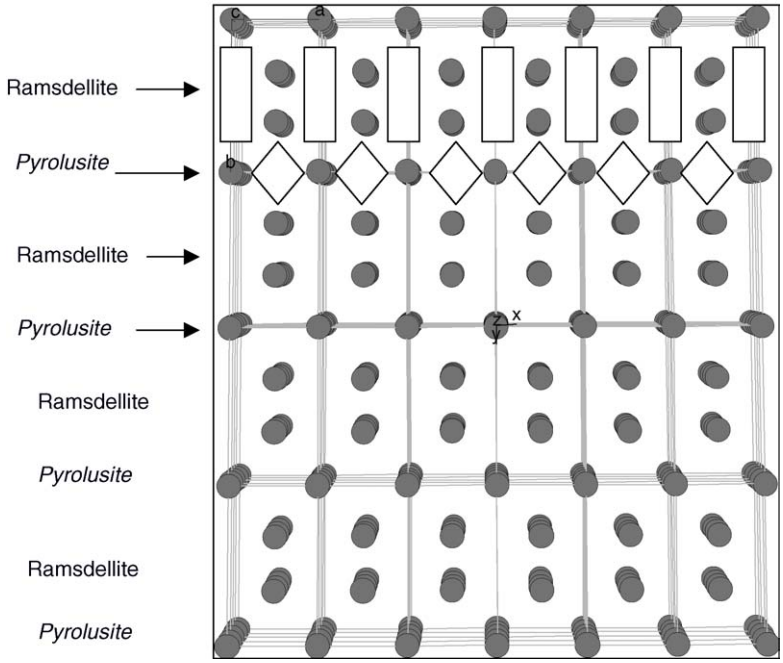

Fig. 16. Conceptual drawing of LiMD structure an an ordered pyrolusite/ramsdellite intergrowth consistent with XRD and CBED results.

dioxide (CDMO) and manganese oxide $LiMn_2O_4$ do not fit into this structural family. CDMO and spinel have a far higher Li content and a different crystal structure based on Li_2MnO_3 rock salt for CDMO and $MgAl_2O_4$ for $LiMn_2O_4$. Moreover, the asymmetric LiMD XRD peak at ~22° 2θ has significant intensity extending to ~20° 2θ. This observation is consistent with the occurrence of the normally forbidden intensity at the ramsdellite 0 0 1 reciprocal lattice position observed in Figs. 10 and 11. We have rationalized this observation by considering the partial ordering of 2×1 and 1×1 tunnels that may occur at high De Wolff defect density. A conceptual drawing of the idealized defect ordering in the LiMD lattice is shown in Fig. 16 below.

4.2. Discharge of LiMD

The SPECS discharges suggest LiMD has a marginally lower capacity than HEMD with an approximate capacity of 250 mAhr g^{-1} compared to about 280 mAhr g^{-1} observed for HEMD. The lower capacity is consistent both with analyses which show a slightly lower Mn(IV) content in LiMD compared to HEMD as well as the Li MAS NMR experiments which show a modest amount of Li in the ramsdellite structure. The SPECS data shows LiMD discharges in an initial reversible step which is shown by the NMR and CBED studies to be initial insertion of lithium into the ramsdellite 1×2 structure leading to a lattice expansion in both a and c directions and formation of a mixed valence Mn (III/IV) product. The NMR studies show that continued lithiation of the ramsdellite results in complete reduction to an Mn (III) product. The second step shown in the SPECS experiment is thought to be the lithiation of the pyrolusite domains of LiMD in a mechanism essentially the same as shown for reduction of the high pyrolusite HEMD material.

5. Conclusion

An ion exchange treatment of electrolytic manganese dioxide with LiOH has been shown to initially replace easily exchangeable surface protons with Li followed by replacement of protons associated with cation vacancy and tightly bound surface sites at higher pH. The drying/heat treatment process that converts protonated EMD to HEMD for use in Li/MnO_2 batteries is modified by the high content of lattice Li and results in formation of a new manganese dioxide phase. The Li in the lattice appears to impede the rearrangement of ramsdellite to pyrolusite and allow instead isolation of the lithiated manganese dioxide phase. Li present on the surface as loosely bound or hydrated ions does not impede this transformation. The transformation is only impeded when Li in tightly bound cation vacancy sites (as formed at high pH) are present. As compared with the spinel phases $LiMn_2O_4$, $Li_2Mn_4O_9$ and $Li_4Mn_5O_{12}$ as well as the lithiated CDMO rock salt phase, the preparative conditions for LiMD allow lithium ion mobility in the lattice [4,12]. The preparative conditions however are not sufficiently severe to lead to a rearrangement of the MnO lattice so the parent ramsdellite/pyrolusite intergrowth is maintained.

LiMD has XRD and CBED patterns consistent with those expected for an ordered intergrowth of ramsdellite and pyrolusite. Inspection of the SPECS discharge data suggests the ratio is about 50% ramsdellite and 50% pyrolusite.

LiMD is easily discharged against metallic lithium and has a capacity slightly less than that of HEMD but discharges at a higher voltage and in a reversible mechanism suggesting better service on high drain discharges.

References

[1] Ikeda, et al., Manganese dioxide as cathodes for lithium batteries, in: Proceedings of the Manganese Dioxide Symposium, vol. 1, Cleveland (1975).
[2] H. Ikeda, M. Hara, S. Narukawa, US Patent 4,133,856 (1979).
[3] Y. Shao-Horn, S.A. Hackney, B.C. Cornilsen, J. Electrochem. Soc. 144 (1997) 3147.
[4] J.C. Nardi, J. Electrochem. Soc. 132 (1985) 1787.
[5] W. Bowden, C. Grey, S. Hackney, X.Q. Yang, Y. Paik, F. Wang, T. Richards, R. Sirotina, ITE Lett. 3 (3) (2002) B1.
[6] Y. Paik, Y. Lee, F. Wang, W. Bowden, C.P. Grey, Materials Research Society Symposium Proceedings, Solid State Chem. Inorg. Mater. III 658 (2001) GG9.11.1.
[7] W. Bowden, M. Capparella, R. Fooksa, US 5,698,176, 16 December 1997.
[8] M. Capparella, W. Bowden, R. Fooksa, US 5,863,675, 26 January 1999.
[9] N. Iltchev, P.A. Christian, W.L. Bowden, P.R. Moses, K. Brandt, US Patent 6,190,800B1 (2001).
[10] P. Christian, O. Mao, US 6,403,257, 11 June 2002.
[11] N. Iltchev, P. Christian, W. Bowden, P.R. Moses, K. Brandt, ITE Lett. 2 (2001) 349.
[12] W. Bowden, R. Sirotina, S. Hackney, ITE Lett. 1 (6) (2000) B27.
[13] W. Bowden, C. Grey, S. Hackney, X.Q. Yang, Y. Paik, F. Wang, T. Richards, R. Sirotina, ITE Lett. 3 (3) (2002) B1.
[14] T. Nohma, Y. Yamamoto, I. Hakane, N. Furakawa, J. Power Sources 51–57 (1992) 39.
[15] T. Nohma, Y. Yamamoto, K. Nishio, I. Hakane, N. Furakawa, J. Power Sources 373–379 (1990) 39.
[16] Y. Chabre, J. Pannetier, Prog. Solid State Chem. 23 (1995) 1–130.
[17] W. Bowden, S. Hackney, R. Sirotina, ITE Lett. 4 (1) (2003) B1.
[18] Y. Paik, J. Osegovic, F. Wang, W. Bowden, C. Grey, J. Am. Chem. Soc. 123 (38) (2001) 9367.